Innovative Air Data System for the Space Shuttle Orbiter

C. David Pruett,* Henry Wolf,† and Michael L. Heck‡
Analytical Mechanics Associates, Inc., Hampton, Virginia
and
Paul M. Siemers III§
NASA Langley Research Center, Hampton, Virginia

The Shuttle entry air data system (SEADS) embodies a flush orifice concept, where, in principle, the Orbiter fuselage functions both as a pitot-static probe and as a differential pressure flow direction sensor. The surface pressure distribution is sampled at an array of orifices on the Orbiter forebody. A digital batch filter, based on a minimum variance criterion, is used to fit a mathematical pressure model to the measured pressures. Forebody pressures are modeled as functions of a four-dimensional "aerodynamic state vector." The filter optimizes the state vector estimate from which standard air data parameters are then derived. Results from simulations, wind tunnel, and flight tests are presented.

Nomenclature

a_j, b_j, c_j = constants, Eq. (12)
Cp = incompressible pressure coefficient, $[(P-P_\infty)/q_\infty]$
$\bar{C}p$ = compressible pressure coefficient, $[(P-P_\infty)/(P_t-P_\infty)]$
f = fineness ratio
$\boldsymbol{h}$ = unit vector normal to surface
H = sensitivity matrix, Eq. (19)
$\boldsymbol{i,j,k}$ = unit vectors along body axes; roll, pitch, and yaw, respectively
k_1, k_2 = constants, Eqs. (8) and (9)
m = scaling function, Eq. (12g)
M = Mach number
P = absolute pressure
q = dynamic pressure, $[\frac{1}{2}\rho V^2]$
R = pressure ratio, $[P_\infty/P_t]$
Re = Reynolds number
S = pressure measurement error covariance matrix, Eq. (23)
t = time
u,v,w = velocity components, Fig. 4
$\boldsymbol{V}$ = velocity vector
$\boldsymbol{X}$ = aerodynamic state vector, Eq. (3)
$\boldsymbol{\Delta X}$ = state update vector, Eq. (22)
$\boldsymbol{y}$ = residual vector, Eq. (20)
α_0 = displacement function, Eq. (12h)
α = angle of attack, Fig. 4
β = angle of sideslip, Fig. 4
γ = ratio of specific heats
ϵ = pressure measurement error
ζ = orifice clock angle, Fig. 3
η = orifice cone angle, Fig. 3
θ = incidence angle, Eq. (7)
Λ = state covariance matrix, Eq. (24)
ρ = density
σ = standard deviation of pressure measurement error

Superscripts

^{0} = initial estimate
$\hat{}$ = apparent state element
^{T} = transpose

Subscripts

i = conditions at orifice i
∞ = freestream conditions
t = total conditions downstream of normal shock

Presented as Paper 81-2455 at the AIAA/SETP/SAE/ITEA/IEEE 1st Flight Testing Conference, Las Vegas, Nev., Nov. 11-13, 1981; submitted Nov. 16, 1981; revision received May 7, 1982.

*Analyst. Member AIAA.
†Senior Scientist. Member AIAA.
‡Senior Analyst.
§Aero-Space Technologist.

I. Introduction

VIRTUALLY every flight vehicle which operates in the continuum atmosphere senses air data by some variant of the pitot-static concept. Flow direction angles, when required in addition to airspeed, Mach number, and pressure altitude, are obtained typically either by flow direction vanes or by differential pressure flow direction sensors. These conventional concepts have been adapted to serve a wide variety of flight vehicles operating over a broad spectrum of flight regimes.

Conventional air data concepts, however, are not adapted readily to entry vehicles. Characteristically, entry vehicles have body contours of large radii of curvature, a design feature necessary to minimize the stagnation point heat transfer rate.[1] Thus, the harsh thermal environment associated with the high hypersonic speeds of entry vehicles prohibits air data sensing vanes or probes which inherently have small radii of curvature or sharp edges.

In the X-15 test program, the thermal constraint to conventional air data sensing was encountered and was solved through the development of the "ball-nose" air data sensor.[2-4] For flight tests at Mach numbers less than 3, the X-15 used a conventional pitot-static nose boom with angle of attack and angle of sideslip flow vanes. For flight tests at Mach numbers in excess of 3 the conventional nose boom was replaced by the ball-nose sensor which consisted of a sphere partly housed in a truncated cone at the forward fuselage station (Fig. 1). A hydraulic servo-mechanism rotated the sphere to maintain pressure differentials between symmetric vertical and lateral flush orifice pairs at null values. Thus, the sphere was positioned in flight such that the center orifice sensed total pressure and the rotation angles of the ball nose

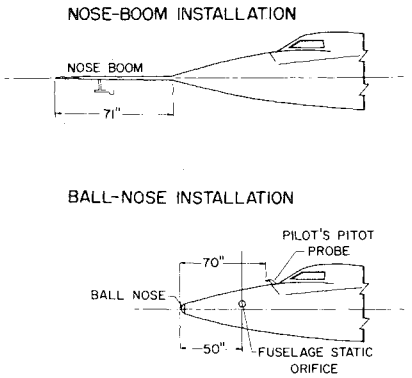

Fig. 1 Conventional and ball nose X-15 air data sensors.

corresponded approximately to flow angles. Static pressure was sensed from two fuselage "static" orifices used in conjunction with the ball nose.

The expanded flight envelope of the Space Shuttle Orbiter, which ranges in Mach number from 0.3 to 27, in angle of attack from −5 to 45 deg, and in temperature to nearly 3000°F, poses air data sensing problems which are uniquely challenging. Existing air data concepts have proven inadequate for such rigorous operational requirements forcing a compromised solution. In the supersonic and subsonic flight of the final minutes of descent, the Orbiter relies on air data provided by two conventional fuselage-mounted differential pressure probes which are deployed at a Mach number of 3.5. In the approximately 25 min of hypersonic flight prior to probe deployment, air data parameters are estimated from the inertially derived navigation state. This situtation is less than ideal, however, since the navigation-derived air data parameters are contaminated by the implicit assumption of zero winds, by a dependency on imprecisely known aerodynamic coefficients, and by inherent navigation state errors. In addition, failure of the navigation solution could jeopardize vehicle controllability.

The Shuttle entry air data system (SEADS) is an experimental system designed to supply reseach quality air data and to meet Orbiter operational air data requirements throughout entry. Like the X-15 ball nose, SEADS is a flush orifice air data system. Unlike the ball nose, SEADS incorporates no mechanical devices but is based on the concept that the fuselage proper, whether symmetrical or not, can be instrumented so as to function both as a pitot-static probe and as a differential pressure flow direction sensor.[5] Specifically, SEADS consists of 20 flush orifices, each routed to a pair of absolute pressure transducers. Fourteen primary orifices form a cruciform array (eight in the plane of symmetry and three symmetric lateral pairs) in the Orbiter's nose cap. Six supplementary orifices are located on the Orbiter forebody aft of the nose cap (Fig. 2).

While the flush orifice air data system is conceptually simple, its implementation in SEADS has developed a computational technique that differs from conventional air data algorithms. The SEADS algorithm, which extracts air data parameters from surface pressure measurements, incorporates a mathematical model of the pressure distribution on the Orbiter forebody and fits this model to observed pressures by means of a digital batch filter. In the language of filter theory, a set of four independent air data parameters comprise the "aerodynamic state vector" $[P_t, P_\infty, \alpha, \beta]$. Either by analytical or empirical techniques, a mathematical model is constructed that represents surface pressures as functions of this state vector. A batch filter then optimizes the state vector estimate by minimizing, in a weighted least squares sense, the differences between the modeled and observed pressures.

This paper formulates the mathematics of air data sensing in the context of filter theory and substantiates experimentally

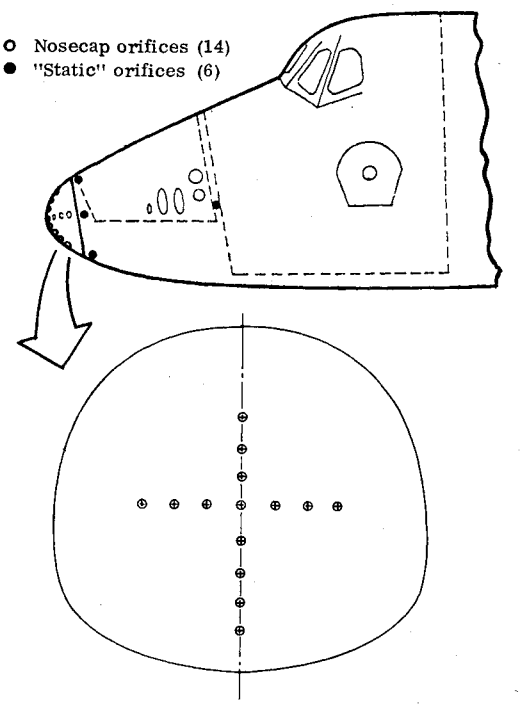

Fig. 2 SEADS orifice configuration.

the resulting algorithm. Section II addresses approaches to pressure field modeling with specific emphasis on the Orbiter forebody pressure model used by SEADS. Section III formulates a simple batch filter for the air data application. Although the complete SEADS configuration has yet to be implemented aboard the Orbiter, the concept and algorithm have been verified using wind-tunnel pressure data, computed simulated Orbiter entry flight data, and subsonic flight data obtained from tests of a SEADS-type system on a KC-135 aircraft. These results are presented in Sec. IV. Section IV concludes by discussing qualitatively the advantages and disadvantages of the flush orifice/digital filter air data concept relative to conventional air data systems.

II. Modeling the Pressure Field

In this section the aerodynamic state vector is defined and approaches are suggested for modeling the pressure distribution on a general body as a function of this four state. The section concludes with a presentation and discussion of the specific Orbiter forebody pressure model applicable to SEADS.

A first step in modeling any physical phenomenon establishes the dimensionality of the problem by identifying the independent variables. For steady, adiabatic, compressible flow, a dimensional analysis argument[6,7] suggests the following generic form for a pressure model in terms of dimensionless groupings:

$$P_i/2q_\infty = G_1(M_\infty, \alpha, \beta, Re, \eta_i, \zeta_i) \tag{1}$$

Here (η_i, ζ_i) could be any pair of dimensionless parameters specifying the location of orifice i on the body. For convenience and consistency with previous references regarding SEADS, η_i and ζ_i are chosen to be the orifice cone and clock angles, respectively, that define the surface normal at orifice i (Fig. 3).

For high Reynolds number flow, the influence of Reynolds number can be neglected for orifices located on the extreme forebody. Thus,

$$P_i = G_2(q_\infty, M_\infty, \alpha, \beta: \eta_i, \zeta_i) \tag{2}$$

The colon separates the "state" variables (those which define flow conditions) from the geometric variables.

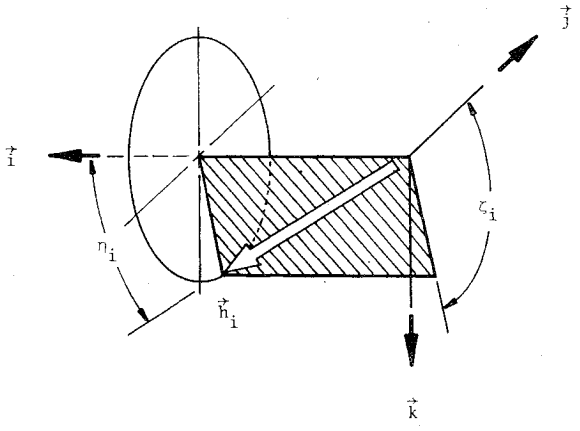

Fig. 3 Orifice cone and clock angles.

Equation (2) establishes the number of independent state variables at four and describes the "aerodynamic state" using the quadruple $(q_\infty, M_\infty, \alpha, \beta)$. This selection of variables, however, is not unique. Equations (13) and (14), which are introduced later, establish relationships between the parameters q_∞, M_∞, P_t, and P_∞, only two of which are independent. For air data sensing in which the primary observables are pressures, it is more natural to describe the state using the pair (P_t, P_∞) rather than (q_∞, M_∞). Therefore, the aerodynamic state vector X is defined to be

$$X \equiv [P_t, P_\infty, \alpha, \beta]^T \tag{3}$$

so that Eq. (2) is recast as

$$P_i = F(X;\ \eta_i, \zeta_i) \tag{4}$$

Thus, the pressure at orifice i is a function of the aerodynamic state defined by Eq. (3) and the position (η_i, ζ_i) of the orifice.

The explicit form of Eq. (4) will depend on body geometry and may be obtained theoretically, empirically, or semiempirically. For simple geometries and/or restricted applications, an adequate theoretical model may exist. For example, modified Newtonian flow theory is used widely to predict pressures for hypersonic flow over blunt convex bodies.[8,9] Equation (5) is the pressure coefficient form of the Newtonian model and Eq. (6) represents an equivalent form in terms of pressures.

$$Cp_i = Cp_i \cos^2\theta_i \qquad (M_\infty \gg 1) \tag{5}$$

$$P_i = (P_t - P_\infty)\cos^2\theta_i + P_\infty \qquad (M_\infty \gg 1) \tag{6}$$

Following Ref. 10 the incidence angle θ_i is defined as the angle between the freestream velocity vector (Fig. 4)

$$\boldsymbol{V}_\infty = |\boldsymbol{V}_\infty|(\cos\alpha\cos\beta\boldsymbol{i} + \sin\beta\boldsymbol{j} + \sin\alpha\cos\beta\boldsymbol{k})$$

and the unit normal vector at orifice i (Fig. 3)

$$\boldsymbol{h}_i = \cos\eta_i\boldsymbol{i} + \sin\eta_i\cos\zeta_i\,\boldsymbol{j} + \sin\eta_i\sin\zeta_i\boldsymbol{k}$$

Thus,

$$\cos\theta_i = \cos\alpha\cos\beta\cos\eta_i + \sin\beta\sin\eta_i\cos\zeta_i + \sin\alpha\cos\beta\sin\eta_i\sin\zeta_i \tag{7}$$

rendering Eq. (6) in the form of Eq. (4).

As a second example, the exact solution for incompressible flow over a spheroid at angle of attack is available from potential flow theory[11] and is a good approximation for compressible flow whenever $M_\infty < 0.4$ (Ref. 12). The pressure coefficient form of the solution is presented next for $\beta = 0$ and orifices in the plane of symmetry.

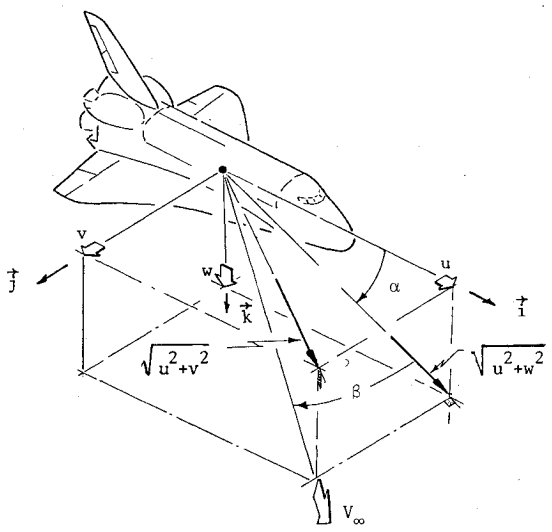

Fig. 4 Body coordinate system.

$$Cp_i = 1 - [k_1\cos\alpha\sin\eta_i - k_2\sin\alpha\cos\eta_i\sin\zeta_i]^2 \qquad (M_\infty \ll 1) \tag{8}$$

The constants k_1 and k_2 depend on the fineness ratio of the spheroid; the limiting values are $k_1 = k_2 = 1.5$ for a fineness ratio of 1 (i.e., a perfect sphere) and $k_1 = 1$, $k_2 = 2$ for a fineness ratio of ∞ (i.e., an infinitely long spheroid). Many fuselage shapes can be approximated roughly as elongated spheroids so that, typically, $k_1 \approx 1$ and $k_2 \approx 2$ (Ref. 13).

Equation (8) will model subsonic compressible flow better if the left-hand side is replaced by the compressible pressure coefficient $\bar{C}p_i$ from which Eq. (9) is derived.

$$P_i = (P_t - P_\infty)\,[1 - (k_1\cos\alpha\sin\eta_i - k_2\sin\alpha\cos\eta_i\sin\zeta_i)^2] + P_\infty \qquad (M_\infty \ll 1) \tag{9}$$

The preceding expression can be generalized for nonzero sideslip resulting in an expression in the general form of Eq. (4).

Equations (6) and (9) represent "global" models in that a single expression defines the pressure distribution at all points (η_i, ζ_i) on a surface.

Alternately the pressure model can be constructed empirically. As an example, the classical air data system calibration is, in essence, construction of an empirical pressure model. Typically, for each orifice i, families of curves depicting the function Cp_i vs α (or β) and M_∞ are generated using wind-tunnel pressure data. If the dependent variable is the compressible pressure coefficient $\bar{C}p_i$, the resulting curves are transformed easily into a set of equations of the form

$$P_i = f_i(X) \tag{10}$$

Equation (10) is the generic form of a "local" pressure model where the subscript i on the right-hand side denotes a unique function corresponding to each orifice.

As a third alternative, a semiempirical model can be formulated wherein an approximate theoretical model is modified on the basis of empirical data.

The specific SEADS forebody pressure model is represented by a global, semiempirical model whose development is described briefly in the following. A fuller exposition is given in Refs. 7, 10, and 14.

SEADS was conceived originally as a hypersonic air data system; appropriately, an early candidate pressure model was that of modified Newtonian theory as defined in Eqs. (6) and (7). As the design matured and both wind tunnel and flight data accumulated, it became apparent that SEADS could provide accurate air data through Orbiter touchdown,

provided that the forebody pressures could be modeled adequately in the supersonic, transonic, and subsonic flight regimes. The model of Eq. (9) with $k_1=1$ and $k_2=2$ was examined as a candidate subsonic model.

Analysis of the modified Newtonian and modified incompressible flow models revealed formal similarities. Both Eqs. (6) and (9) can be rendered in the form

$$P_i=P_t[(1-R)f(\alpha,\beta,\eta_i,\zeta_i)+R] \tag{11}$$

where $R\equiv P_\infty/P_t$. As the pressure ratio R is a function of the freestream Mach number M_∞ [Eq. (13)], Eq. (11) makes explicit a dependence of the pressure distribution on the Mach number. In the limit as $M_\infty\to 0 (R\to 1)$, $P_i\to P_\infty$ for all orifices. Thus, both the modified Newtonian and modified incompressible models are consistent with the physical situation when there is no motion.

Moreover, both the modified incompressible and modified Newtonian models predict the same pressure distribution for an elongated spheroid at zero incidence; that is, for $k_1=1$ and $k_2=2$ in Eq. (9), Eqs. (6) and (9) are identical whenever $\alpha=\beta=0$.

For nonzero angle of attack, there is a further similarity between the two models. For the assumption of $\beta=0$ and small α, the modified incompressible flow model with $k_1=1$ and $k_2=2$ and the modified Newtonian flow model are equivalent in all first-order terms with one important distinction; the term containing α in Eq. (9) is scaled by a factor of 2 (arising from $k_2=2$). Thus, if an "apparent" or "Newtonian" angle of attack $\hat{\alpha}$ is introduced by the relation $\alpha=0.5\,\hat{\alpha}$, the modified Newtonian theory predicts the correct pressures for an elongated spheroid at incidence for $M_\infty\ll 1$. Reference 7 arrives at a similar conclusion without presupposing small α.

Fitting the modified Newtonian model to subsonic wind-tunnel pressure data confirms the linear relationship between apparent angle of attack $\hat{\alpha}$ and true angle of attack α. Moreover, comprehensive wind-tunnel testing reveals that the linear relationship $\alpha=m(\hat{\alpha}+\alpha_0)$ holds at any Mach number where m varies from 0.5 to 1.0 as a function of Mach number. The "displacement function" α_0, also a function of Mach number, arises due to the vertical asymmetry of the Orbiter which induces displacement of the stagnation streamline at zero angle of attack. A similar linear relationship holds between the apparent and true sideslip angles although the corresponding displacement function β_0 is zero because of the lateral symmetry of the Orbiter.

Based on these analytical and empirical considerations, an Orbiter forebody pressure model valid over the entire speed range may be constructed. It is summarized in Eq. (12).

$$P_i=P_t[(1-\hat{R})\cos^2\hat{\theta}_i+\hat{R}] \qquad |\hat{\theta}_i|<65\text{ deg} \tag{12a}$$

$$\hat{R}=a_0+a_1R+a_2R^2+a_3R^3$$

$$a_0=0; \qquad a_1+a_2+a_3=1 \tag{12b}$$

$$R=P_\infty/P_t \tag{12c}$$

$$\cos\hat{\theta}_i=\cos\hat{\alpha}\cos\hat{\beta}\cos\eta_i+\sin\hat{\beta}\sin\eta_i\cos\zeta_i$$

$$+\sin\hat{\alpha}\cos\hat{\beta}\sin\eta_i\sin\zeta_i \tag{12d}$$

$$\alpha=m(\hat{\alpha}+\alpha_0) \tag{12e}$$

$$\beta=m\hat{\beta} \tag{12f}$$

where

$$m=b_0+b_1R \tag{12g}$$

$$\alpha_0=c_0+c_1R \tag{12h}$$

The cubic function $\hat{R}$ of Eq. (12b) generalizes the pressure ratio R resulting in better agreement between the modeled and actual pressure data in the intermediate Mach number ranges. The restrictions that $a_0=0$ and that a_1, a_2, and a_3 sum to unity insure that $\hat{R}=R$ in the limiting case of hypersonic $(R\to 0)$ and incompressible $(R\to 1)$ flows.

The function m in Eqs. (12e-g) is the scaling function which interprets the apparent angle of attack $\hat{\alpha}$ (or sideslip $\hat{\beta}$) depending on the Mach number (in practice, as a function of R). A value of $m=1$ at $R=0$ is consistent with Newtonian flow theory and a value of $m=0.5$ at $R=1$ is consistent with the incompressible flow Eq. (9) where $k_1=1$ and $k_2=2$. The displacement function α_0 is computed as a function of R according to Eq. (12h).

In practice, the sequence of computations is as follows. Using Eqs. (12a) and (12d), the filter estimates the apparent state $\hat{X}\equiv[P_t,\hat{R},\hat{\alpha},\hat{\beta}]^T$. The pressure ratio R then is obtained from $\hat{R}$ using Eq. (12b) and, subsequently, true angles of attack and sideslip are computed using Eqs. (12e-h). Static pressure is obtained from R and P_t by means of Eq. (12c).

Once the aerodynamic state vector has been determined, the additional air data parameters M_∞ and q_∞ are obtained conventionally.[15] Mach number M_∞ is computed from Eq. (13a) in the supersonic flight regime or Eq. (13b) in the subsonic flight regime.

$$R\equiv P_\infty/P_t=\left[\frac{2}{(\gamma+1)M_\infty^2}\right]^{\frac{\gamma}{\gamma-1}}\left[\frac{2\gamma M_\infty^2-(\gamma-1)}{\gamma+1}\right]^{\frac{1}{\gamma-1}}$$

$$M_\infty>1$$
$$(R<0.53)$$

Rayleigh pitot formula (13a)

$$R=P_\infty/P_t=\left[1+\frac{\gamma-1}{2}M_\infty^2\right]^{-\frac{\gamma}{\gamma-1}} \qquad M_\infty\le 1 \quad (R\ge 0.53) \tag{13b}$$

Equation (13b) is solved explicitly for M_∞, but Eq. (13a) requires iteration. Dynamic pressure q_∞ is derived from P_∞ and M_∞ as $q_\infty=(\gamma/2)P_\infty M_\infty^2$, or, in practice,

$$q_\infty=(\gamma/2)P_tRM_\infty^2 \tag{14}$$

For small $R(M_\infty\gg 1)$, the product RM_∞^2 is nearly constant (~ 0.54) so that it is possible to obtain q_∞ very accurately even though gross errors may exist in P_∞ and M_∞.

Although the pressure model of Eqs. (12) was developed specifically for the Orbiter forebody geometry, it is applicable to a general class of elongated blunt bodies with lateral (but not necessarily vertical) symmetry. In general, the constants a_j, b_j, and c_j depend on the particular geometry and can be determined through wind-tunnel investigation or, conceivably, through pressure data generated by numerical solution of the flow equations. Once the body pressure distribution has been modeled as a function of the aerodynamic state, the principles of filter theory are readily adapted to air data sensing.

III. Batch Filter

In the last two decades, digital filtering has attained widespread use and acceptance in the aerospace industry. Filters are routinely used for state estimation in navigation, guidance, and control systems.[16] Here this theory is adapted to the task of estimating the aerodynamic state vector from a set of pressure measurements.

If $f_i(X)$ models the pressure at orifice i as a function of the aerodynamic state defined by Eq. (4), the observed pressure at orifice i can be represented by

$$p_i=f_i(X)+\epsilon_i \tag{15}$$

where ϵ_i is the error in the observed pressure P_i, assumed to have zero mean. Suppose that at time t, n pressue observations are available. Define the following n vectors:

$$P \equiv \begin{bmatrix} P_1 \\ P_2 \\ \cdot \\ \cdot \\ P_n \end{bmatrix}, f \equiv \begin{bmatrix} f_1(X) \\ f_2(X) \\ \cdot \\ \cdot \\ f_n(X) \end{bmatrix} \quad \epsilon \equiv \begin{bmatrix} \epsilon_1 \\ \epsilon_2 \\ \cdot \\ \cdot \\ \epsilon_n \end{bmatrix} \tag{16}$$

The relationship between the observation vector P and the state vector X can now be represented as the vector equation

$$P = f(X) + \epsilon \tag{17}$$

Generally, f is a nonlinear function of X. Linearization of the vector function f results in the following approximation to Eq. (17).

$$P = f(X^\circ) + \left[\frac{\partial f}{\partial X}\right]_{X=X^\circ} \Delta X + \epsilon \tag{18}$$

where X° is an a priori state estimate and ΔX is the vector $X - X^\circ$ denoted the "update vector." For brevity, define the "sensitivity matrix" H as

$$H \equiv \left[\frac{\partial f}{\partial X}\right]_{X=X^\circ} \tag{19}$$

and the residual vector y

$$y \equiv P - f(X^\circ) \tag{20}$$

where H is an $n \times 4$ matrix readily obtained by differentiation of the vector function f. Equation (18) can now be written succinctly as

$$y = H\Delta X + \epsilon \tag{21}$$

The best linear minimum variance unbiased estimate for the update vector ΔX is computed according to the following.[17]

$$\Delta X = (H^T S^{-1} H)^{-1} H^T S^{-1} y \tag{22}$$

where S is the observation error covariance matrix; i.e.,

$$S \equiv E[\epsilon\epsilon^T] = \begin{bmatrix} \sigma_1^2 & & & & 0 \\ & \sigma_2^2 & & & \\ & & \cdot & & \\ & & & \cdot & \\ & & & & \cdot \\ 0 & & & & \sigma_n^2 \end{bmatrix} \tag{23}$$

assuming measurement errors to be uncorrelated. Equation (22) is identical to a weighted least squares formulation when the weighting matrix W is given by $W = S^{-1}$ (Ref. 17).

The a priori state estimate X° may lie outside the region in which f is approximated adequately by a linear function. It then is desirable to refine the initial state estimate X° using a new value computed by $X^\circ + \Delta X$. The process from Eq. (19) to the new $X^\circ + \Delta X$ value is repeated. The entire iteration procedure is equivalent to an application of the four-dimensional analog of the Newton-Raphson method; hence, convergence is quadratic from a sufficiently good initial estimate X° (Ref. 18). Since a good first estimate is always available (for example, from a previous converged solution) few iterations are needed. All air data parameters at time t are derived from the final (converged) four-state estimate.

A by-product of the filter algorithm is the optimal estimate of the state covariance matrix Λ given by

$$\Lambda = (H^T S^{-1} H)^{-1} \tag{24}$$

This quantity, which arises naturally in Eq. (22), is a measure of the uncertainty in the estimate of the update ΔX (i.e., $\Lambda = E[\Delta X, \Delta X^T]$) and is a function both of the observation error covariance S and of the sensitivity of the model to changes in the state.

Table 1 Pressure model constants

	WT	SIM	FADS
a_1	2.03	1	1
a_2	−2.57	0	0
a_3	1.55	0	0
b_0	0.71 ($R \geq 0.46$) 0.93 ($R < 0.46$)	1	0.5
b_1	−0.18 ($R \geq 0.46$) −0.66 ($R < 0.46$)	−0.5	0
c_0, deg	−0.50 ($R \geq 0.09$) +0.50 ($R < 0.09$)	0	0
c_1, deg	5.25 ($R \geq 0.09$) −6.25 ($R < 0.09$)	0	0
n	14	14	18

IV. Results and Conclusions

Results

Although SEADS has yet to be implemented aboard the Orbiter, the flush orifice/digital filter air data concept has been verified through extensive wind-tunnel testing (WT), computer simulations (SIM), and flight testing of the flush air data system (FADS) similar to SEADS aboard a conventional subsonic transport aircraft. The results presented herein were obtained using the batch filter algorithm represented by Eq. (22), the generalized forebody pressure model of Eqs. (12), and a set of measured (WT, FADS) or simulated (SIM) orifice pressures.

The particular values of the constants a_j, b_j, and c_j used in Eqs. (12) depend upon the geometry of the test article and are summarized in Table 1. For the wind-tunnel testing, the test articles were two high-fidelity Orbiter forebody models for which the constants a_j, b_j, and c_j were derived empirically using a selected subset of the total wind-tunnel pressure data set. The test article for the flush air data system flight test was a KC-135 aircraft. The constants shown in Table 1 for the FADS test are assumed values.¶ For the computer simulation, the constants reflect a simplified pressure model which is used both to generate simulated pressure data and to process the data.

The wind-tunnel, simulation, and flight test results presented in this section represent the performance of "stand-alone" flush orifice/digital filter air data implementations where the orifice array is comprised solely of n (refer to Table 1) nosecap orifices; that is, "static" orifices aft of the nosecap are not included. It is to be expected then (as results will

¶Unfortunately, insufficient wind-tunnel data were available to evaluate properly the geometry-dependent coefficients for the KC-135 implementation. The assumed values are based on the approximations that the KC-135 geometry at the nosecap is spheroidal, that the fuselage fineness ratio is very large ($f \gg 1$), and that $M_\infty \ll 1$. This latter approximation, in particular, induces considerable error in the FADS test results.

Table 2 Typical wind tunnel results (14 orifice SEADS configuration)

Reference state						Recovered state						
P_t, (PSF)	α, deg	β, deg	P_∞, (PSF)	M_∞ (ND)	q_∞, (PSF)	P_t (PSF)	α, deg	β, deg	P_∞, (PSF)	M_∞, (ND)	q_∞, (PSF)	e_{rms}
2984	0.2	0.0	2856	0.25	125	2985	0.3	0.0	2886	0.22	98	0.06
1994	6.0	−3.9	1786	0.40	200	1994	6.5	−3.6	1823	0.36	166	0.13
2530	−2.0	0.0	1984	0.60	500	2536	−2.1	0.1	2005	0.59	487	0.32
1699	15.9	−1.9	1114	0.80	499	1709	15.9	−1.3	1016	0.89	570	0.75
1414	8.0	6.1	791	0.95	500	1419	8.1	6.2	766	0.98	516	0.51
1258	18.0	2.0	590	1.10	500	1269	17.8	2.5	545	1.17	525	1.00
1229	4.0	6.0	542	1.15	502	1230	4.1	5.9	579	1.10	488	0.47
1195	14.0	6.0	496	1.20	500	1203	14.3	6.2	486	1.22	509	0.79
1501	2.0	−0.1	553	1.30	655	1506	2.3	−0.1	568	1.28	652	0.55
1113	12.0	−1.9	365	1.40	501	1118	12.5	−1.5	353	1.43	508	0.84
1221	7.2	−0.1	358	1.50	563	1229	7.8	0.3	348	1.53	571	0.73
842	30.0	5.0	116	2.30	428	856	30.1	5.7	126	2.21	432	0.94
695	0.0	0.0	59	2.96	362	705	0.2	0.1	57	3.04	368	0.73
576	15.0	0.0	36	3.50	304	588	14.9	−0.1	37	3.46	310	0.83
408	25.0	5.0	15	4.63	218	415	25.3	5.1	16	5.08	222	0.76

$n = 1361$	mean error	= −0.4%	−0.15 deg	−0.17 deg	−0.7%	1.2%	4.3% ($M_\infty \le 1$) 1.8% ($M_\infty > 1$)
	standard deviation =	0.5%	0.25 deg	0.19 deg	5.0%	5.2%	10.9% ($M_\infty \le 1$) 3.3% ($M_\infty > 1$)
	maximum error	= 2.8%	−0.93 deg	−0.78 deg	−20.0%	16.3%	23.5%

confirm), that static pressure P_∞ will be poorly determined relative to the other state elements. Consequently, the accuracies of M_∞ and q_∞, which are derived in part from P_∞ will be somewhat degraded. When the pressure model is expanded to include static orifices, total system performance will be enhanced significantly.

Wind Tunnel

The development program for the SEADS has included an extensive series of subsonic/transonic,[19] supersonic, and hypersonic wind-tunnel tests that is nearly complete at the present time. In total, over 3000 frames of pressure data have been obtained using two high-fidelity Orbiter forebody models at Mach numbers ranging from 0.25 to 10.3. The outcome of this test program has been twofold. The generalized pressure model of Eqs. (12) has been developed through a combination of theoretical analysis and wind-tunnel experimentation where the form of the model has been derived primarily from theoretical considerations and the values of the constants a_j, b_j, and c_j specific to the Orbiter geometry have been obtained by empirical methods (see Table 1). In addition, the wind-tunnel test program has provided a wealth of pressure data from which approximately 1400 frames of the highest resolution data have been selected for verification of the SEADS concept and algorithm.

Table 2 summarizes the ability of the SEADS filter algorithm to recover wind-tunnel reference state values given only 14 nosecap pressure measurements. The first six columns display tunnel reference conditions in p_t, α, β, P_∞, M_∞, and q_∞. The next six columns present the corresponding recovered state parameters obtained from filtering on the surface pressures. Because of the large volume of data available, it is possible to list only typical results in Table 2. However, the mean and standard deviation of the errors, for 1361 data frames, are given.

The discrepancy between the reference and recovered state values reflect the contributions of several error sources which include: 1) uncertainties in tunnel reference conditions, 2) pressure measurement errors, 3) pressure modeling errors, 4) uncertainties in orifice cone and clock angles, and 5) local effects of surface irregularities.

The last column in Table 2 is a "goodness of fit" indicator which is the root-mean-square pressure residual error normalized to total pressure P_t; i.e.,

$$e_{rms} \equiv \frac{1}{P_t}\left[\frac{\sum_{i=1}^{n}(P_i - f_i)^2}{n}\right]^{1/2} \tag{25}$$

The indicator e_{rms} is a measure of the combined magnitude of fitting error incurred from sources 2, 3, 4, and 5 given earlier. Typically, the root-mean-square residual error is less than 1% of total pressure although some degradation of fit occurs at high angles of attack and at transonic Mach numbers.

Simulation

In contrast to the wind-tunnel results presented previously, the results obtained through computer simulation reflect the potential accuracy of SEADS in the presence of single source error and as a function of time t during entry. Since Eqs. (12) are used both to generate pressures and to interpret pressures, the single error source is the vector ϵ of random errors which is added to the simulated pressure vector $\boldsymbol{P}$ [see Eq. (17)]. At each time t, a new error vector is generated.

Figure 5 presents, as a function of time from entry insertion minus 5 min, the errors in angle of attack and the Mach number and relative errors in total and dynamic pressures compared to the corresponding reference state parameters. The reference state values vs time, which are superimposed in Fig. 5, have been extracted from a nominal Shuttle entry trajectory tape[20] and are considered exact for the simulation. The error in sideslip $\Delta\beta$ is similar to angle-of-attack error and is not shown. The 3σ error envelope, which also is superimposed on the angle-of-attack error and relative total pressure error plots, has been derived from the covariance matrix as defined by Eq. (24).

At any time t, the state errors shown in Fig. 5 depend solely on the magnitude and direction of the error vector ϵ. Thus, the noise model used to generate ϵ has been designed to be as consistent as possible with SEADS hardware characteristics.

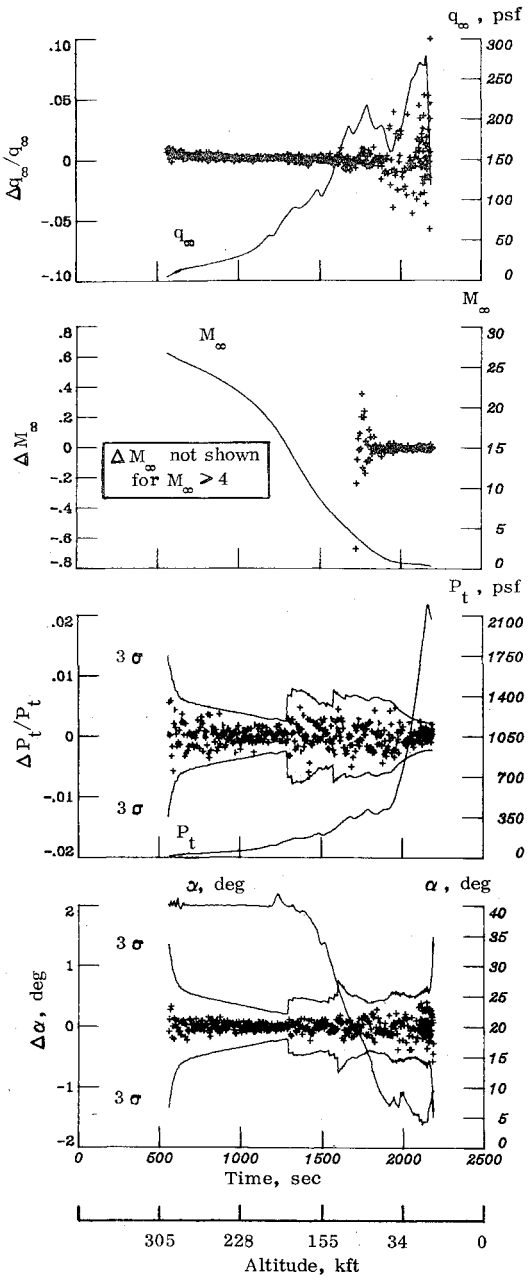

Fig. 5 Predicted SEADS uncertainties.

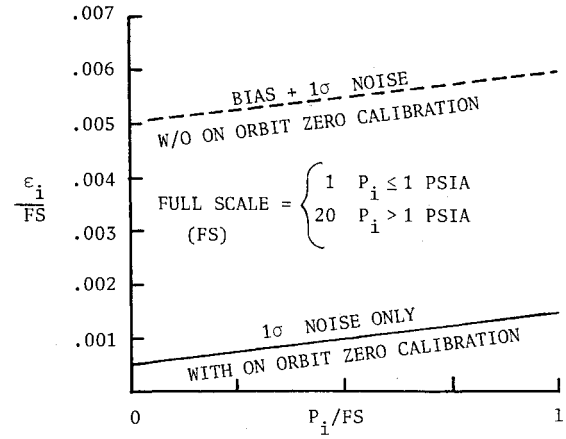

Fig. 6 Simulation noise model.

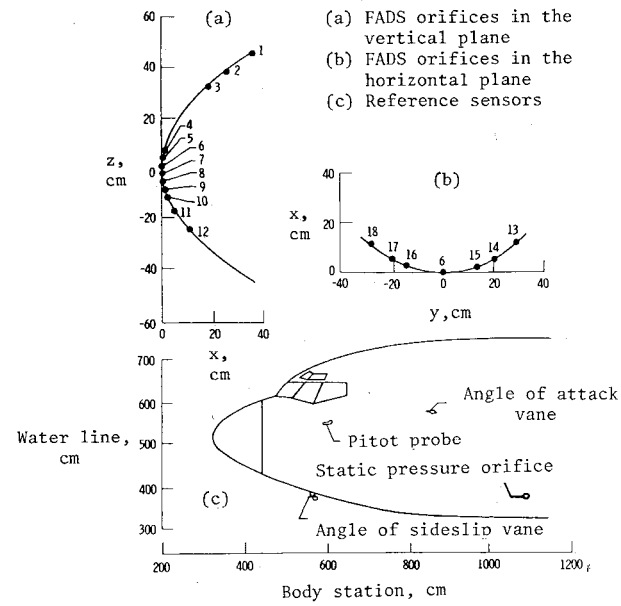

Fig. 7 Locations of FADS orifices and reference air data sensors.

Each component ϵ_i of ϵ is a random error (no bias) whose standard deviation is computed according to Fig. 6. In the SEADS implementation, transducer bias is minimized by the taking of an on-orbit zero pressure measurement prior to entry. Note that SEADS incorporates a dual transducer configuration at each orifice which is reflected in Fig. 6.

A few comments are in order concerning the behavior of the errors in Fig. 5. The discontinuities in angle of atack and total pressure errors occurring at $t \sim 1300$ s result from the onset of transitions from low-range (0-1 psia) to high-range (0-20 psia) transducers at which time the magnitude of the error vector ϵ is large relative to the magnitude of the pressure vector $\boldsymbol{P}$. The rapid degradation in angle-of-attack and total-pressure accuracies for $t < 600$ is explained similarly; the magnitude of ϵ is large in a relative sense because pressures, at this extreme altitude, are quite low. The rapid degradation in Mach number accuracy in the hypersonic flight regime is a manifestation of the Mach number independence principle[21] whereby, as M_∞ becomes large (in practice, for $M_\infty > 4$), the pressure distribution is nearly independent of M_∞. The sharp increase in angle-of-attack uncertainty as $M_\infty \to 0$ arises due to the physical singularity at $M_\infty = 0$ at which $P_i = P_\infty$ (for all i) independently of attitude. These latter three phenomena are the consequences of physical singularities and are not peculiar to the SEADS configuration or algorithm.

Flush Air Data System

In order to assess the subsonic performance of a SEADS-type system, an 18 orifice array was tested on a KC-135 aircraft[22] (Fig. 7). The flight pressure data, obtained at 1 Hz, were recorded and processed postflight by the SEADS filter algorithm. Figure 8 compares the angle of attack, total pressure, Mach number, and dynamic pressure obtained from the flush air data system to the corresponding state parameters provided by the reference air data system. The ship standard air data system, which is used as the reference, consists of fuselage mounted angle-of-attack and sideslip flow vanes, a total pressure probe, and two symmetric fuselage static ports. Unfortunately, error sources present in this flight test make it difficult to quantify the performance of the FADS. These are as follows.

1) The "off the shelf" pressure model is only approximate; i.e., the constants a_j, b_j, and c_j given in Table 1 are assumed values rather than values derived from wind-tunnel investigation for the KC-135 geometry.

2) Large uncertainties (± 3 deg) exist in the orifice cone (η_i) and clock (ζ_i) angles.

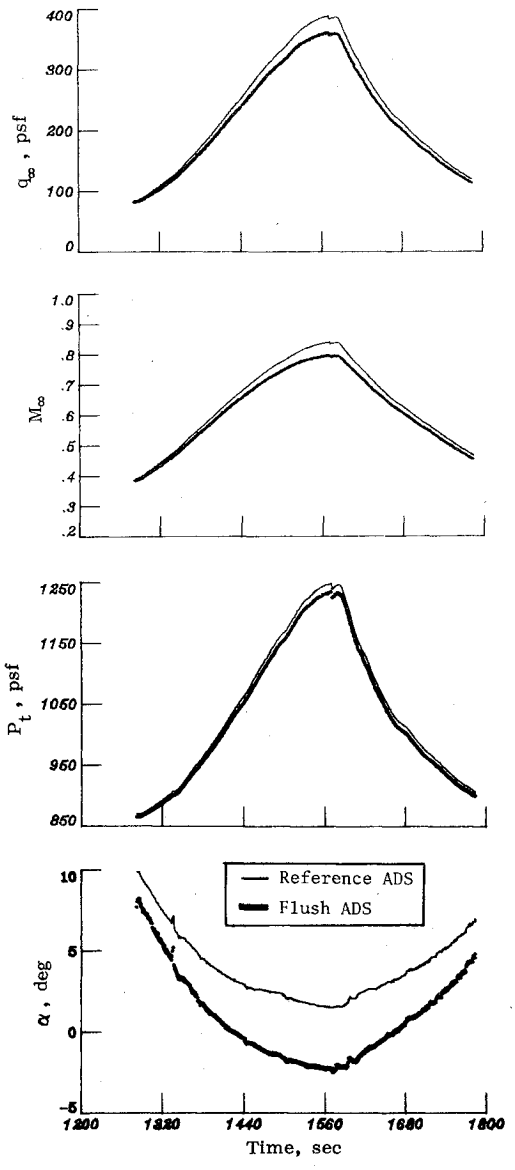

Fig. 8 Comparison of conventional and flush orifice air data systems.

3) Large uncertainties exist in the reference parameters α and β. Despite these limitations, it can be seen that the FADS responds to all the dynamics exhibited by the reference air data system with no apparent lag, and that the FADS could be calibrated easily to a true reference state.

Although the data were processed in a postflight mode, there appears to be no impediment to using the filter algorithm for real-time applications. Convergence was obtained in, at most, three iterations using the previously converged state as an initial estimate.

Qualitative Results

A presentation of the results obtained from the implementations of the flush orifice/digital filter concept would be incomplete without a few comments regarding the qualitative behavior of the batch filter algorithm relative to conventional air data algorithms. A distinguishing characteristic of the filtering algorithm is that all observations project onto the state space. In an air data context, this is to be interpreted that every pressure measurement participates to some degree in the determination of every state element. This is in marked contrast to a classical pressure-based air data sensing scheme whereby, typically, only that orifice (or orifice pair) demonstrating the greatest sensitivity to the change in a given state variable is allowed to participate in the determination of that variable.

A corollary to the trait that "all observations project" is that of inherent redundancy. Because all pressure observations participate in the computation of each state variable, the loss of a single observation or even several observations need not be catastrophic provided that there are a sufficient number of well-spaced orifices. In particular, the 14 orifice SEADS has demonstrated exceptional fault tolerance; accurate results have been obtained (from simulated and wind-tunnel pressure data) in the presence of both single and multiple orifice failures. In contrast, the loss of the total pressure measurement in a conventional pitot-static system is catastrophic. Thus, multiple probes are required to provide redundancy in a conventional system.

Unlike conventional air data algorithms, the digital filter algorithm permits data editing. Any measurement "outlier" P_k is automatically flagged within the filtering algorithm as having a residual y_k which is large relative to the others. It is a simple matter then to eliminate outliers using statistical tests. The computation is repeated subsequently using a reduced observation set.

A disadvantage of the filtering algorithm is that computation time is probably longer than in conventional algorithms. Unfortunately, no real-time basis of comparison currently exists. However, the results of computer simulations indicate that the digital filtering algorithm is fast enough for real-time air data sensing applications.

Because the relationship between the pressures and the aerodynamic state vector is nonlinear, the filter algorithm inherently is iterative. Conventional algorithms may or may not contain iterative routines. In the wind tunnel, simulation, and FADS test cases of the filter algorithm, convergence was reliable and rapid (typically three or fewer iterations) even in the presence of gross errors in the initial state vector estimate.

Summary and Conclusions

The unique air data sensing problems posed by the Space Shuttle Orbiter and the limitations of conventional air data systems demand innovation in air data concepts. The experimental SEADS combines two such innovations each of which is an extension of proven concepts. The flush orifice concept has evolved from the pitot-static sensor, the hemispherical head differential pressure sensor, and the ball nose. The digital filtering algorithm implemented in SEADS is the natural adaptation to air data sensing of a technology widely used in navigation, guidance, and control systems.

The Shuttle Entry Air Data System and the concepts it embodies have been verified qualitatively and quantitatively through extensive analysis, wind-tunnel testing, computer simulation, and flight testing. Based on these results the following conclusions are presented.

1) SEADS is a viable "stand-alone" air data system capable of meeting Orbiter operational air data requirements throughout entry.

2) The digital filter algorithm is suitable either for postflight analysis or real-time flight control.

3) The geometry of the orifice arrangement used in SEADS and the nature of the digital filter algorithm result in an air data system which is highly fault tolerant.

4) The flush orifice/digital filter air data system is general in nature and applicable to a wide variety of flight vehicles.

Acknowledgments

This research was supported by NASA Langley Research Center through Contract NAS1-16245.

References

[1] Fay, J.A. and Riddell, F.R., "Theory of Stagnation Point Heat Transfer in Dissociated Air," AVCO Research Lab., June 1956.

[2]Fischel, J. and Webb, L.D., "Flight Informational Sensors, Display, and Space Control of the X-15 Airplane for Atmospheric and Near-Space Flight Missions," NASA TN D-2407, Aug. 1964.

[3]Cary, J.P. and Keener, E.R., "Flight Evaluation of the X-15 Ball-Nose Flow Direction Sensor as an Air-Data System," NASA TN D-2923, July 1965.

[4]Larson, T.J. and Webb, L.D., "Calibration and Comparison of Pressure-Type Airspeed-Altitude Systems of the X-15 Airplane from Subsonic to High Supersonic Speeds," NASA TN D-1724, Feb. 1963.

[5]Siemers, P.M. III and Larson, T.J., "Space Shuttle Orbiter and Aerodynamic Testing," *Journal of Spacecraft and Rockets,* Vol. 16, July-Aug. 1979, p. 227.

[6]Shames, I.H., *Mechanics of Fluids,* McGraw-Hill, New York, 1962, pp. 188-204.

[7]Pruett, C.D., "Determination of Angle of Attack by the Shuttle Entry Air Data System in Supersonic Flow," Master's Thesis, The University of Virginia, Charlottesville, Va., 1980.

[8]Love, E.S., Woods, W.C., Rainey, R.W., and Ashby, G.C. Jr., "Some Topics in Hypersonic Body Shaping," AIAA Paper 69-181, 1969.

[9]"Bodies of Revolution," *Handbook of Supersonic Aerodynamics, Section 8,* Vol. 3, The Johns Hopkins University Applied Physics Laboratory, Silver Spring, Md., NAVWEPS Rept. 1488, 1961.

[10]Wolf, H. and Eades, J.B. Jr., "Analysis of the Shuttle Air Data System," Analytical Mechanics Associates, Inc., Hampton, Va., AMA Rept. 77-20, 1977.

[11]Thwaites, B., *Incompressible Aerodynamics,* Clarendon Press, Oxford, 1960, p. 395.

[12]Zucrow, M.J. and Hoffman, J.D., *Gas Dynamics,* Vol. I, John Wiley & Sons, New York, 1976, p. 132.

[13]Jones, R.T., Ed., *Classical Aerodynamic Theory,* NASA Ref. Pub. 1050, 1979, pp. 151-159.

[14]Pruett, D. and Wolf, H., "Postflight Data Reduction for Shuttle Entry Air Data System Part I: Hypersonic/Supersonic," Analytical Mechanics Associates, Inc., Hampton, Va., AMA Rept. 80-28, 1980.

[15]Ames Research Staff, *Equations, Tables, and Charts for Compressible Flow,* NACA TR 1135, 1953.

[16]Schmidt, S.F., "The Kalman Filter: Its Recognition and Development for Aerospace Applications," *Journal of Guidance and Control,* Vol. 4, Jan.-Feb. 1981, pp. 4-7.

[17]Tapley, B.D., "Statistical Orbit Determination Theory," presented at NATO Advanced Study Institute in Dynamical Astronomy, Cortina d'Ampezzo, Italy, 1972.

[18]Ortega, J.M. and Poole, W.G. Jr., *An Introduction to Numerical Methods for Differential Equations,* Pitman Publishing Inc., Marshfield, Mass., 1981, p. 140.

[19]Matt, R.G., "Wind Tunnel Tests of the Shuttle Entry Air Data System (SEADS) at Mach Numbers from 0.25 to 1.50," Calspan Field Services, Inc., Arnold Air Force Station, Tenn., AEDC-TSR-81P22, May 1981.

[20]"Flight Tape Description," NASA Johnson Space Flight Center, Houston, Tex., Memo, FM17 (79-120), 1979.

[21]Hayes, W.D. and Probstein, R.F., *Hypersonic Flow Theory,* Academic Press, New York, 1979, pp. 24-26.

[22]Larson, T.J., and Siemers, P.M. III, "Subsonic Investigation of an All Flush Orifice Air Data System," presented at 1980 Air Data Systems Conference, Colorado Springs, Colo., May 1980.